REPORT DOCUMENTATION PAGE

AFRL-SR-AR-TR-05-

0442

1. REPORT DATE (DD-MM-YYYY)	2. REPORT TYPE	3. DATES COVERED (From - To)
March 1, 2005	Final Report	August 1, 2002 – February 28, 2005

4. TITLE AND SUBTITLE

IRIS Diagnoses of Man-made and Naturally-occurring Ionospheric Plasma Turbulence

5a. CONTRACT NUMBER

5b. GRANT NUMBER
F49620-01-1-0481

5c. PROGRAM ELEMENT NUMBER

6. AUTHOR(S)

Min-Chang Lee

5d. PROJECT NUMBER

5e. TASK NUMBER

5f. WORK UNIT NUMBER

7. PERFORMING ORGANIZATION NAME(S) AND ADDRESS(ES)

Plasma Science and Fusion Center
Massachusetts Institute of Technology
77 Massachusetts Avenue
Cambridge, Massachusetts 02139

8. PERFORMING ORGANIZATION REPORT NUMBER

9. SPONSORING / MONITORING AGENCY NAME(S) AND ADDRESS(ES)

Air Force Office of Scientific Research
875 North Randolph Street, Suite 325, Room 3112
Arlington, Virginia 22203
Contractor Manager: Dr. Kent L. Miller

10. SPONSOR/MONITOR'S ACRONYM(S)
AFOSR/NE

11. SPONSOR/MONITOR'S REPORT NUMBER(S)

12. DISTRIBUTION / AVAILABILITY STATEMENT

Approved for public release;
Distributed unlimited

13. SUPPLEMENTARY NOTES

14. ABSTRACT

Radio wave experiments have been conducted at Arecibo, Puerto Rico and Gakona, Alaska together with numerical analyses aimed at investigating man-made and naturally-occurring ionospheric plasma turbulence. Research progress and results reported include the following. (1) Ionospheric ELF and VLF experiments in Alaska discover that a horizontal Hertzian magnetic dipole (HMD) with a radius of about 7 km at an altitude around 70 km is responsible for the generation of ELF/VLF waves. (2) Numerical analyses of ELF and VLF wave generation show that the modulation scheme using the half-wave rectified wave is the most efficient one to generate signals at the modulation frequency and second harmonic, confirming our theoretical predictions. (3) Theoretical study of ionospheric HF heating experiments finds that the dominant factors, determining the number of cascade lines in the radar-detected spectrum of HF enhanced plasma lines (HFPLs), include the ion to electron temperature ratio, Ti/Te, the background plasma inhomogeneity scale length, and the heating wave field intensity. (4) The very intense ionospheric plasma turbulence observed over Arecibo, Puerto Rico on December 26, 2004 was possibly triggered by the tsunami-induced gravity waves, propagating from Sumatra, Indonesia to Puerto Rico about 23 hours after the occurrence of a $M_W = 9.2$ earthquake.

15. SUBJECT TERMS

Ionospheric plasma turbulence; ELF/VLF wave generation; electrojet current; HF heating experiments; Hertzian magnetic dipole; tsunami-induced gravity waves

16. SECURITY CLASSIFICATION OF:			17. LIMITATION OF ABSTRACT	18. NUMBER OF PAGES	19a. NAME OF RESPONSIBLE PERSON
a. REPORT	b. ABSTRACT	c. THIS PAGE			Min-Chang Lee
Unclassified	Unclassified	Unclassified		20	19b. TELEPHONE NUMBER (include area code) 617-253-5956

IRIS Diagnoses of Man-made and Naturally-occurring
Ionospheric Plasma Turbulence

Table of Contents

IRIS Diagnoses of Man-made and Naturally-occurring Ionospheric Plasma Turbulence

(F49620-01-1-0481, August 01, 2001 – February 28, 2005)

Under the sponsorship of Air Force Office of Scientific Research (AFOSR), we have been conducting radio wave experiments at Gakona (Alaska) and Arecibo (Puerto Rico), and theoretical and numerical analyses of ELF/VLF wave generation and interactions with ionospheric plasmas. This work is aimed at investigating man-made and naturally occurring ionospheric plasma turbulence. Research progress and results of these sponsored programs are reported as follows.

(1) Ionospheric ELF and VLF Experiments in Alaska

Controlled ELF and VLF wave-generation experiments, using the HAARP (High-frequency Active Auroral Research Program) radio facility, have been conducted at Gakona, Alaska. These experiments are aimed at (1) understanding how man made ELF/VLF waves can affect the space plasma environment, and (2) developing novel and efficient communication schemes using high quality of ELF and VLF radio signals. Two graduate students carried out the experiments for their thesis research, under the guidance of the Principal Investigator. Two senior thesis/UROP (Undergraduate Research Opportunity Program) students also participated in the experiments. Our experiments have led to the discovery that ELF/VLF waves, induced by high power amplitude-modulated HF waves, are actually radiated from a horizontal Hertzian magnetic dipole (HMD) with a radius of about 7 km, rather than a horizontal Hertzian electrical dipole (HED), at an altitude around 70 km. This discovery advances our understanding of high power radio wave interaction with electrojet currents, and guides us further to explore novel controllable communications schemes in space.

The experimental illustrated in Figure 1 shows that electrojet currents (EJ) were illuminated by HF waves, which were amplitude-modulated at a frequency in the range of ELF (0.3 - 3 KHz) or VLF (3 - 30 KHz). The amplitude-modulated HF waves could subsequently radiate ELF or VLF waves as artificial antennas. An HF receiver and an ELF/VLF receiver were set up to record the transmitted HF modulation and radiated ELF/VLF signals, respectively. The HF and ELF/VLF receivers were GPS-synchronized to allow us to determine the relative phase of the HF and VLF waves. The HF transmitter was operated in two different modes, one used a modulation frequency sweep, and the other a heater beam angle sweep. Based on these setup and operations, we could determine the "effective altitude" of the electrojet radiation source and deduce the "absolute phase response" of the heater-electrojet system. Observation were made for both radiated modes at fundamental and harmonic frequencies.

Displayed in Figure 2 are the expressions for the radiated ELF/VLF wave magnetic field underneath the heated patch of the ionosphere for two different types of dipoles. In the case of the Hertzian electric dipole (HED), the perturbed currents close around the sides of the heated region. In the Hertzian magnetic dipole (HMD) case, perturbed currents close over the top of the heated region. In both cases the radiated wavelength is assumed

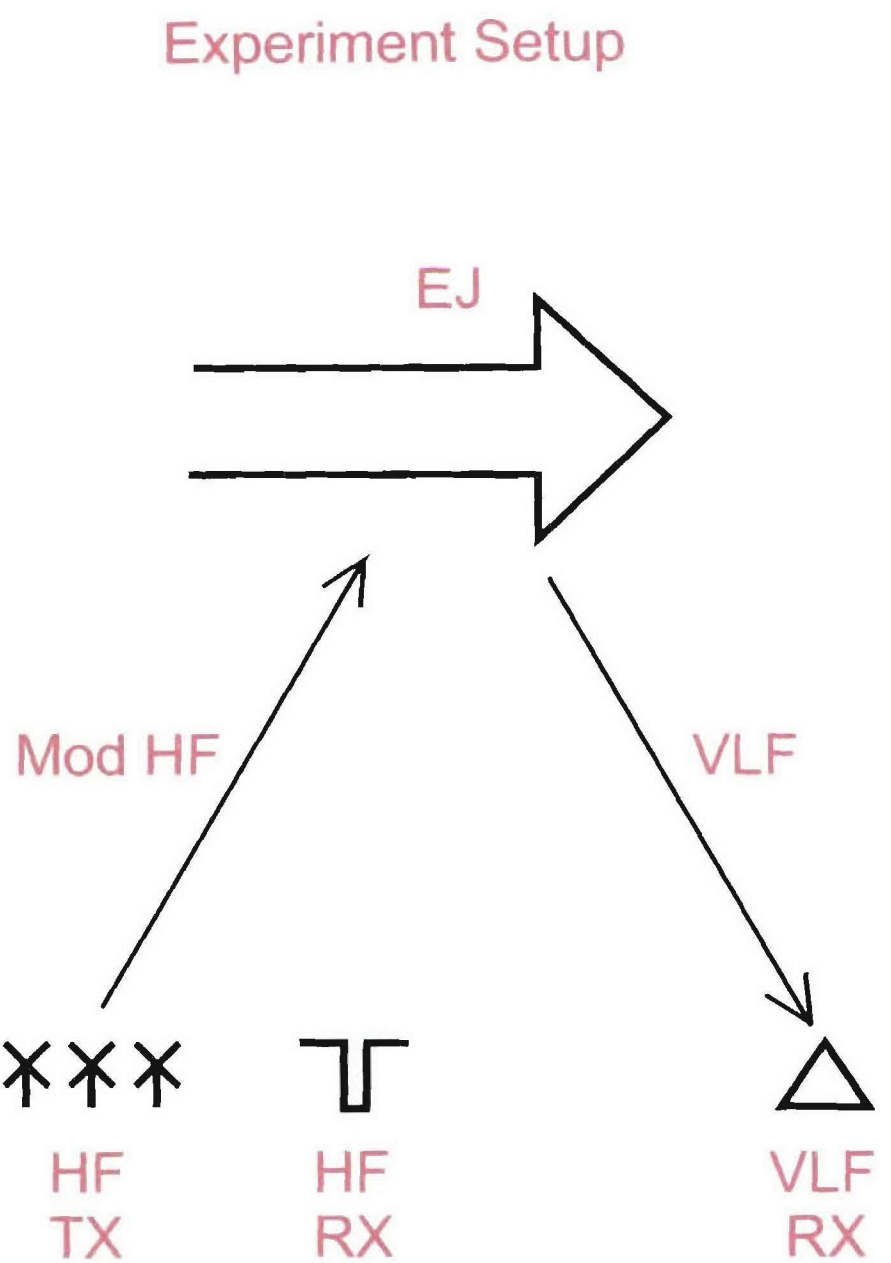

Figure 1.

Horizontal electric dipole (HED)

$$H_\phi = -ikIl\frac{e^{ikr}}{4\pi r}\left[1+\frac{i}{kr}\right]\sin\theta$$

$\Longrightarrow$ 1 zero, 1 pole, and linear phase

Horizontal magnetic dipole (HMD)

$$H_\theta = -k^2IA\frac{e^{ikr}}{4\pi r}\left[1+\frac{i}{kr}+\left(\frac{i}{kr}\right)^2\right]\sin\theta$$

$\Longrightarrow$ 2 zeros, 1 pole, and linear phase

Figure 2.

to be large compared to the size of the dipole. The HMD expression has one more zero than the HED expression and thus the HMD radiation will lead the HED radiation by 90 degrees. Plotted in Figure 3 is the phase of the ELF/VLF radiation received on the ground relative to the phase of the transmitted modulation. The two lines indicate the theoretical phase for a horizontal electric dipole (HED) and a horizontal magnetic dipole (HMD). The circles are the experimental points, which appear to favor the HMD.

Due to the exp(ikz) linear phase factor in the radiation expressions, the asymptotic slope of the phase versus frequency curves shown in Figure 4 gives the altitude of the ELF/VLF radiation source (assuming free space radiation). The theoretical phase for three different altitudes is plotted as lines. The experimental points suggest that the radiation source has an apparent altitude of 71 km. When the radiated ELF/VLF wavelength is of comparable size to the current loop, an additional Bessel function factor appears in the HMD radiation formula (compare to the expression in Figure 2). The Bessel function flips sign when its argument is 3.83. This sign flip appear as a jump of 180 degrees in the measured phase of the radiation if a sufficiently high modulation frequency is used. ELF/VLF radiation has been observed up to 35 kHz. Indeed, when the phase of the fifth harmonic of the modulation is plotted, a phase jump appears at about 25 kHz. This frequency corresponds to an effective current loop radius of 7.3 km. The detailed description and analysis of these ionospheric ELF and VLF experiments are presented in R.J. Riddolls' Ph.D. dissertation entitled " Structure of the polar electrojet antenna" [MIT, 2004].

(2) Numerical Analysis of ELF and VLF Wave Generation

In addition to aforementioned experiments, we have conducted numerical studies of ELF/VLF wave generation by amplitude-modulated HF heating waves. The details of this work is reported in a paper entitled "Experimental and numerical studies on ELF/VLF wave generation by amplitude-modulated HF heating waves" by Kuo et at. [Phys. Scr. T., 67, 448, 2003]. This paper presents numerical results for the comparison with our theoretical predictions [Kuo and Lee, Geophys. Res. Lett., 20, 189, 1993] as well as our experimental data, regarding the dependency of generation efficiency on the HF heating wave modulation scheme and frequency. In our Alaska experiments we examined three heating wave modulation schemes: (1) rectangular wave, (2) sine wave, and (3) half-wave rectified wave. Our experimental results indicate that the modulation scheme using the half-wave rectified wave is the most efficient one to generate signals at the modulation frequency and second harmonic, confirming our theoretical predictions. It should be pointed out that ELF/VLF radiation processes are contributed by both the near field and the far field of the antenna current. The resonant effect on the wave field intensity, in the resonator formed by the conducting ground and the lower ionosphere, is also included in our theoretical model. Our numerical simulation results show the dependency of ELF or VLF radiation intensity on the modulation frequency, in a good agreement with our experimental measurements for all the three modulation schemes.

(3) Theoretical Study of Ionospheric HF Heating Experiments

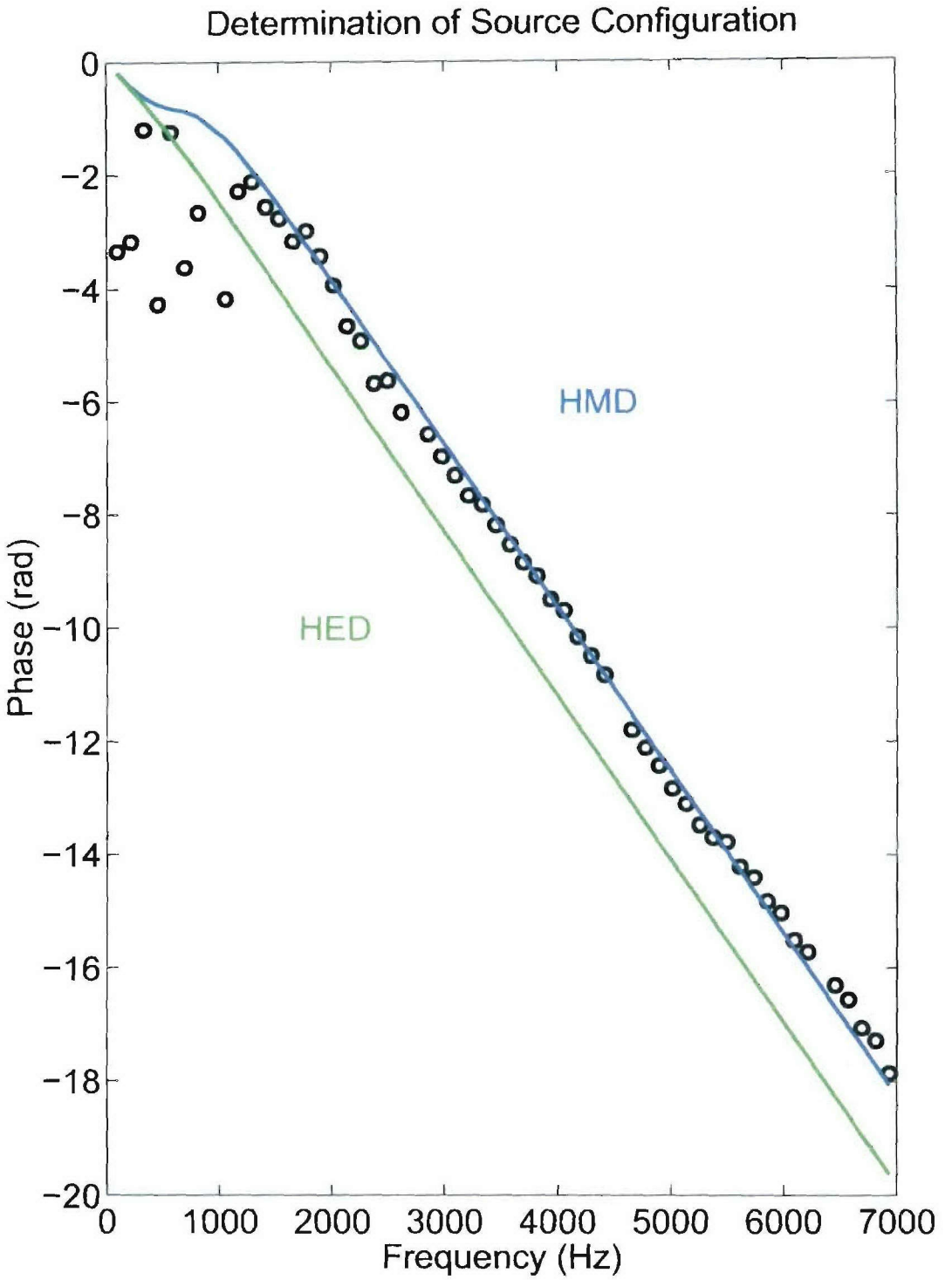
Determination of Source Configuration
0
−2
−4
−6
−8
−10
−12
−14
−16
−18
−20
Phase (rad)
HMD
HED
0
1000
2000
3000
4000
5000
6000
7000
Frequency (Hz)

Figure 3.

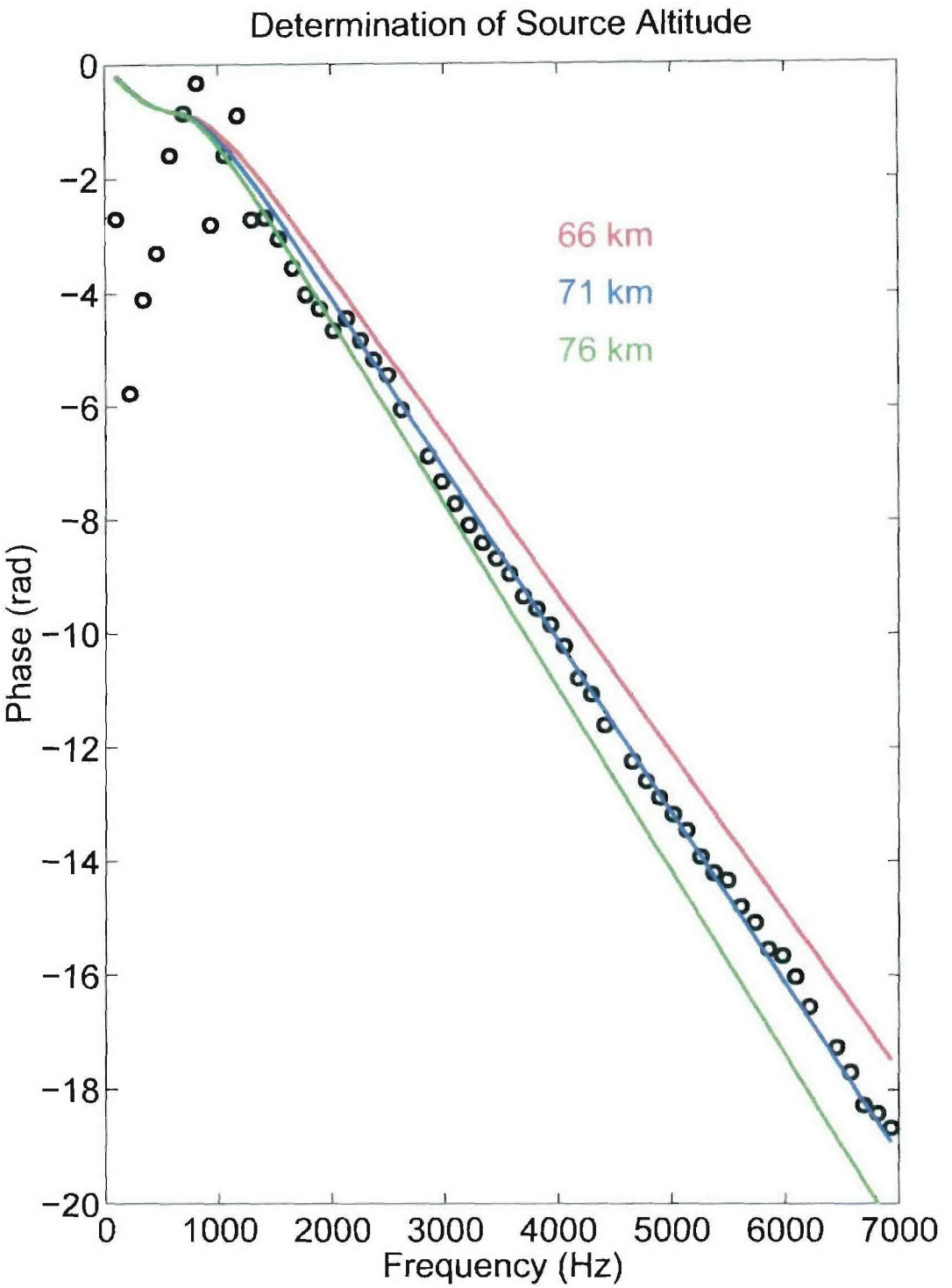
Determination of Source Altitude
66 km
71 km
76 km
Phase (rad)
Frequency (Hz)
0
−2
−4
−6
−8
−10
−12
−14
−16
−18
−20
0
1000
2000
3000
4000
5000
6000
7000

Figure 4.

We have examined theoretically the cascade spectrum of HF enhanced plasma lines generated in HF heating experiments and reported the results in a paper by Kuo and Lee [J. Geophys. Res., 110, A1, 1309, 2005]. Analyzed in this paper is the cascade spectrum of Langmuir waves, which are the high-frequency sideband of the parametric decay instability or oscillating two-stream instability excited by an O mode HF heating wave. It involves the decay of a Langmuir pump wave into a Langmuir sideband and an ion acoustic wave, which is heavily damped by ion Landau damping. Both resonant and nonresonant cascade processes are considered. The nonresonant cascade of Langmuir waves proceeds at the same location and is severely hampered by the frequency mismatch effect, because the decay wave is a driven ion mode oscillating at considerably lower frequency than that of the ion acoustic wave. In contrast, the resonant cascade, which takes place at different resonant locations to minimize the frequency mismatch effect, has to overcome the propagation loss of the mother Langmuir wave in each cascade step. The resonant cascade has a lower threshold, but the cascade lines spread over a range of altitude. The dominant factors, which determine the number of cascade lines in the radar-detected spectrum of HF enhanced plasma lines (HFPLs), include the ion to electron temperature ratio, Ti/Te, the background plasma inhomogeneity scale length, and the heating wave field intensity. The proposed process can be a reasonable basis for explaining the radar-measured cascade spectrum of Langmuir waves (i.e., HFPLs) in Arecibo and Tromso heating experiments.

(4) Ionospheric Plasma Turbulnce Triggered by Tsunami-induced Gravity Waves over Arecibo, Puerto Rico

In a paper recently submitted to Journal of Geophysical Research, we report results of ionospheric plasma measurements conducted at the Arecibo Observatory between 20:00 and 24:00 local time (LT) on December 25 and 26, 2004 using the 430 MHz incoherent scatter radar (ISR) and ionosonde. Initially, the ISR transmitted using a rotating and tilted line feed to help find turbulent regions of the local ionosphere. After identifying active regions, diagnoses were conducted with the radar stationary and pointing toward zenith. The ISR detected different ionospheric behaviors during the vertical-transmission periods on the consecutive, magnetically quiet nights. On the night of December 25 ionosphere descended smoothly and spread F signatures faded. Over the course of an hour on the following evening the bottomside ionosphere rose by 50 km, inducing plasma density irregularities and intensified spread F, then descended. We interpret this behavior as a response to a gravity wave propagating above Puerto Rico. Experiments on December 26 were conducted about a day after an MW = 9.2 earthquake launched the disastrous tsunami across the Indian Ocean. We suggest that coupling at the tsunami sea-air interface created gravity waves that reached the ionosphere and propagated along the great circle between Sumatra and Puerto Rico. The gravity wave's velocity field caused plasma in the local ionosphere to rise, seeding bottomside irregularities via generalized Rayleigh-Taylor instability. Because this work has not been published yet, we highlight the key results as follows.

Arecibo Experiments

We first report experimental results acquired between 20:00 and 24:00 LT on December 25 [00:00 to 04:00 UT on December 26], 2004. Figure 5 (a) illustrates the general geometry of the experiments on both nights. The primary instruments were the 430 MHz ISR and an ionosonde located at the Arecibo Observatory. Measurements from the ISR are reported power (P_b) backscattered from the altitude range 100 to 600 km. This quantity depends on the ionospheric plasma density (N_e) and the ratio of electron and ion temperatures (T_e/T_i), in the form $P_b \propto N_e /(1 + T_e/T_i)$. The ionosonde at Arecibo is a vertically transmitting, swept-frequency HF radar that operates between 1 and 20 MHz. Output ionograms are plots of radar reflection heights as functions of frequency (corresponding to the local ionospheric plasma density). Diffuse echoes on ionograms called spread F, indicate the presence of plasma turbulence in the bottomside of the ionospheric F region, associated with density irregularities with scale lengths ranging from tens of centimeters to hundreds of kilometers. Although the spread F phenomenon has been observed for more than half a century [Booker and Wells, 1938], the source mechanisms producing the mid-latitude spread F often remain mysterious at locations, such as Arecibo. The $\mathbf{E} \times \mathbf{B}$ and Perkins instabilities have been invoked to explain spread F occurrences at Arecibo [e.g., Behnke, 1979; Basu et al., 1981].

(A) Rotating ISR Operations

Initially the ISR line feed (i.e., transmitter) was tilted 15° from vertical and rotated clockwise from 0° to 360°, and then counter-clockwise from 360° to 0°, as illustrated in Figure 5(b). Note that if the line feed was in the northwest sector, radar waves were emitted toward the southeast. On average 360° rotations took ~15.77 minutes. The radar beam has an angular width of 0.16°, when transmitting at 430 MHz. The beam-width of the nearby ionosonde is ~ ±45° and covers the entire region scanned by the ISR. Ionograms were recorded every 5 minutes. The ionosonde and ISR operated simultaneously to monitor the occurrence of spread-F due to bottomside density irregularities and the evolution of ionospheric distributions in the entire F layer.

Figure 6 shows ISR and ionograms data recorded between 20:00 and 24:00 LT on December 25, 2004. The upper panel of Figure 6 shows a range-time-intensity (RTI) plot of backscatter power displayed in a relative intensity format that ranges from 0 to 1. The maximum value of radar backscatter power in a data file is set at an intensity of 1. The color bar to the right of the RTI indicates the intensity of P_b. Dark areas on the RTI plot indicate regions of weak P_b where N_e was low. Seven blank stripes reference radar data gaps that occurred as operational modes changed. During ISR power-mode operations pulses of 52 μs duration were transmitted every 10 ms. They consisted of a 13-baud Barker code with 4 μs bauds, resulting in 600 m range resolution, with an integration of 200 pulses for 2 s time resolution.

The middle panel of Figure 6 shows the temporal variation of the height-integrated backscattered power $\int P_b(t)\, dh$ along the radar beam between 150 and 600 km altitude.. Below the local time axis are alternating arrows: → and ← indicating times of clockwise and counter-clockwise radar rotation, respectively. Since we expect no significant

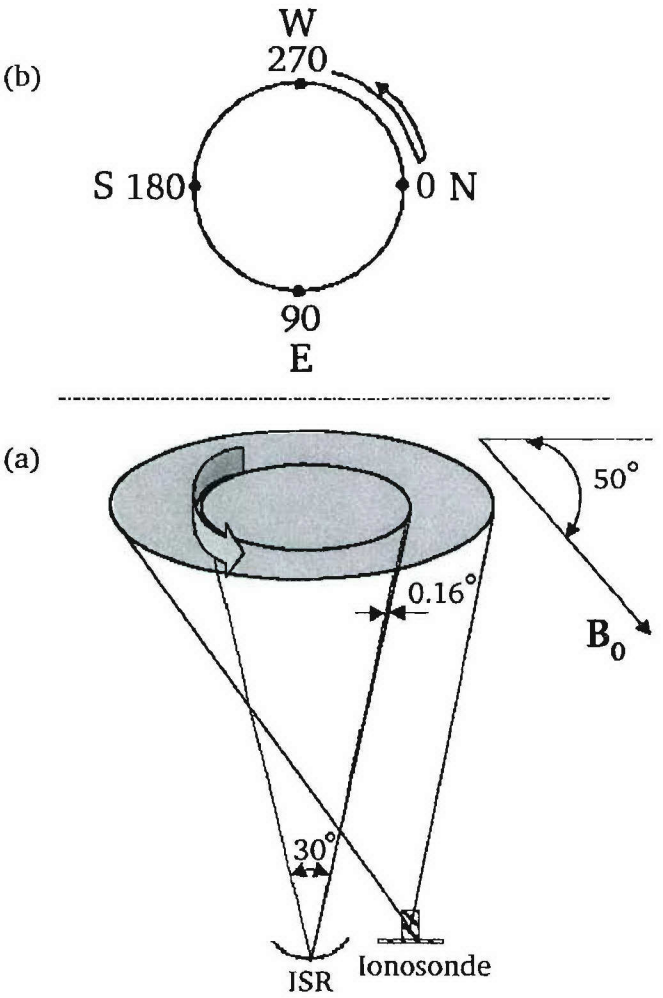

Figure 5. (a) Illustration of Arecibo ionosonde and ISR radiating from the rotating, tilted line feed, to diagnose ionospheric plasma turbulence. (b) Top view of the cone traced by the rotating, tilted line feed of the radiating ISR.

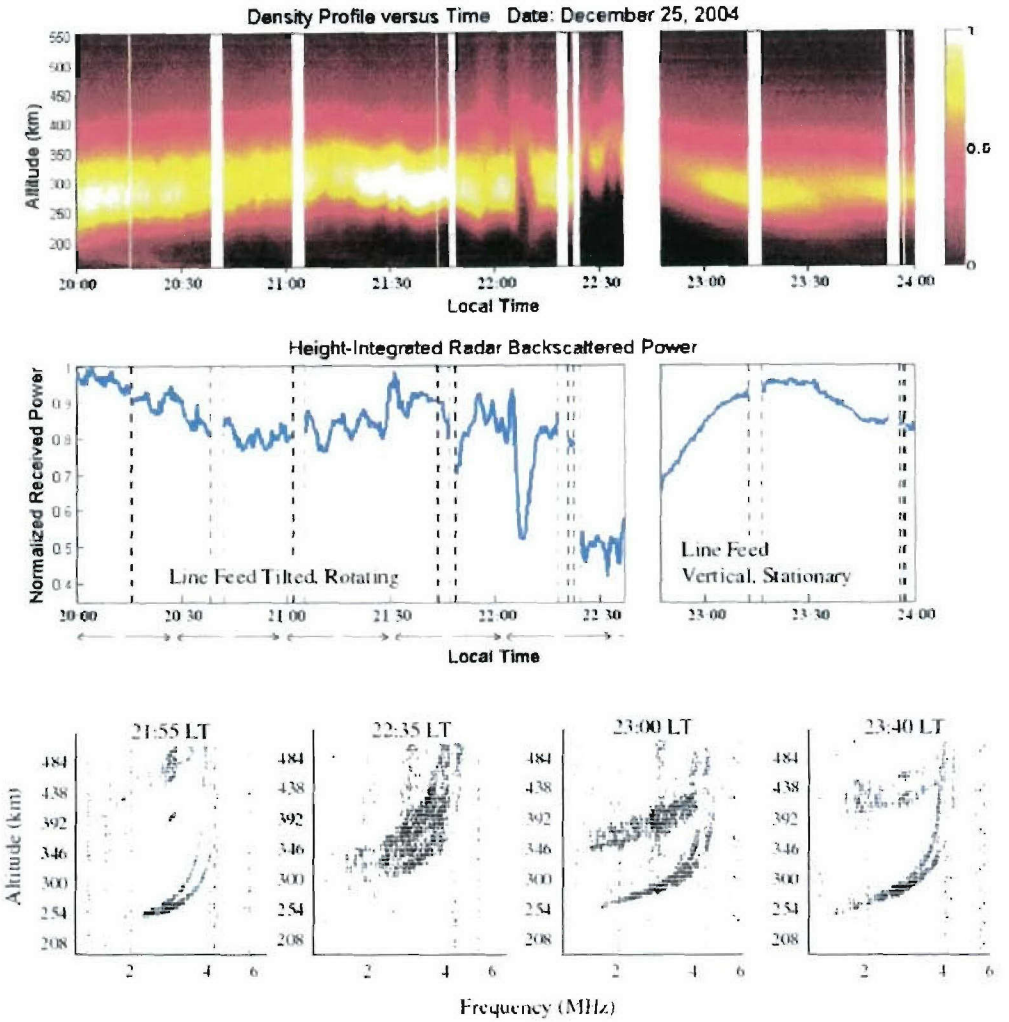

Figure 6. (Top panel) The range-time-intensity (RTI) plot of radar backscatter power recorded on December 25, 2004 from 20:00:00 to 24:00:00 local time (LT). (Middle panel) The corresponding normalized, dimensionless height-integrated radar backscatter power ($\sim$ TEC) as a function of local time. (Bottom panel) Four sampled ionograms recorded during the experiments, to monitor the corresponding ionospheric plasma conditions.

change in T_e/T_i at mid latitudes over this altitude range, $\int P_b(t)\, dh$ is proportional to $\int N_e(t)\, dh$, the total electron content (TEC). The bottom row of Figure 6 contains four ionograms that are representative of conditions in the periods of acquisition.

During the initial phase of the rotating line-feed operations, 20:00 to 22:05 LT, both the RTI plot and height-integrated backscattered power show rather quiet ionospheric plasma conditions. Notable plasma density structures and reductions appear in Figure 6 near 22:06 and after 22:25 LT. Spread F echoes accompanied the irregularities (cf. 21:55 LT ionogram). To observe the ionospheric depletion and associated irregularities more closely, we stopped rotating line feed operation at 22:36:42 LT. It took ~15 minutes to bring the ISR line feed to a stationary, vertical position.

(B) Stationary ISR Operations

Immediately after the stationary radar line feed operations began at 22:47:07 LT, the density reductions/irregularities weakened and spread F echoes faded. From 22:42:29 LT to the end of the experiments at 24:00:00 LT, the radar and ionosonde detected no significant ionospheric turbulence that appeared in Figure 6 following the fall and rise of the F layer.

We next consider Arecibo experimental results obtained between 20:00 and 24:00 LT on December 26 [00:00 to 04:00 UT, December 27], 2004. Figure 7(a) shows three plasma-density profiles recorded between 20:00 and 24:00 local time (LT) on December 26, 2004. Figure 7(b) show the experimental geometry and a schematic representation of a rising plasma depletion indicated by the three plasma-density profiles. As on the previous day, the 430 MHz ISR operations began with the line feed tilted and rotating.

(A) Rotating ISR Operations

The upper panel of Figure 8 shows normalized RTI backscatter powers recorded between 20:00: and 23:20 LT in the same format as Figure 6. Deep ionospheric plasma depletions are prominent features in ionospheric regions probed by the rotating 430 MHz radar beam especially near 20:53:28 LT and 21:27:39 LT. Note that since the radar beam rotation changed from clockwise to counter-clockwise rotation at 21:32:37, the two peaked values in the $\int P_b(t)\, dh$ trace labeled A and B, represent the same plasma structure sampled before and after the reversal. The same ionospheric structure A/B was probed by the rotating radar beam at different times and had changed location due to ionospheric drift, as illustrated in Figure 9. This together with Figure 8 can be used to explain how the rotating radar beam encountered different depleted ionospheric regions as follows.

The RTI plot and discrete density profiles allows determinations of the times when the radar beam intercepted the structures A and B. To within an accuracy of 10 s the radar beam encountered A and B at 21:25:18 and 21:33:21 LT, respectively. The rotation reversal occurred at 21:32:37 LT, or 441 s after encountering A. The radar beam encountered B 44 s after the reversal. Thus, 483 s is the approximate time between the

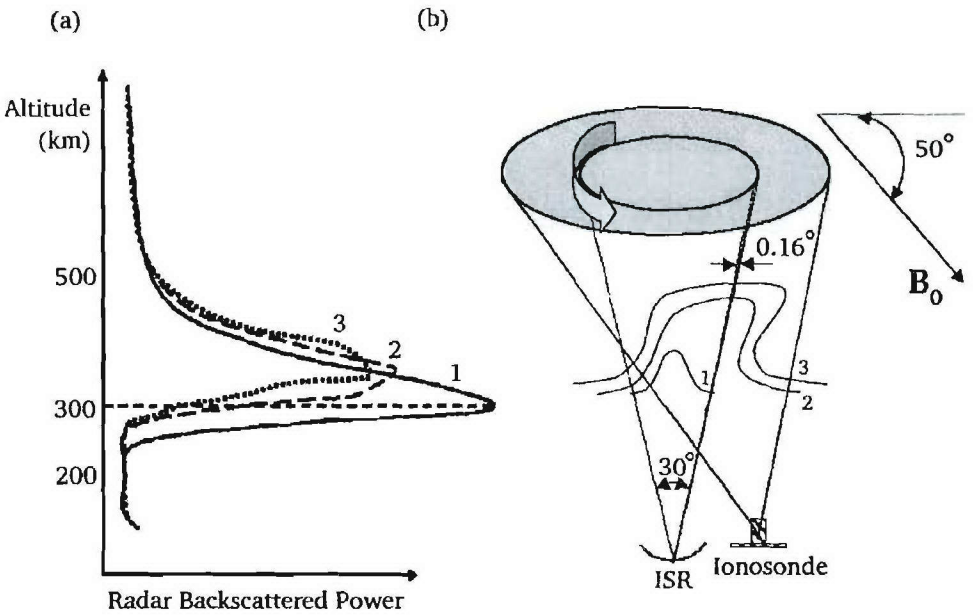

Figure 7. (a) Shapes of three ionospheric density profiles recorded on December 26, 2004 at 21:54:12, 22:00:54 and 22:09:17 local time (LT), respectively, during the development of ionospheric density depletion and the evolution of a rising plasma bubble. (b) Illustration of Arecibo ionosonde and ISR radiating from the rotating, tilted line feed, to monitor the development of ionospheric plasma bubbles.

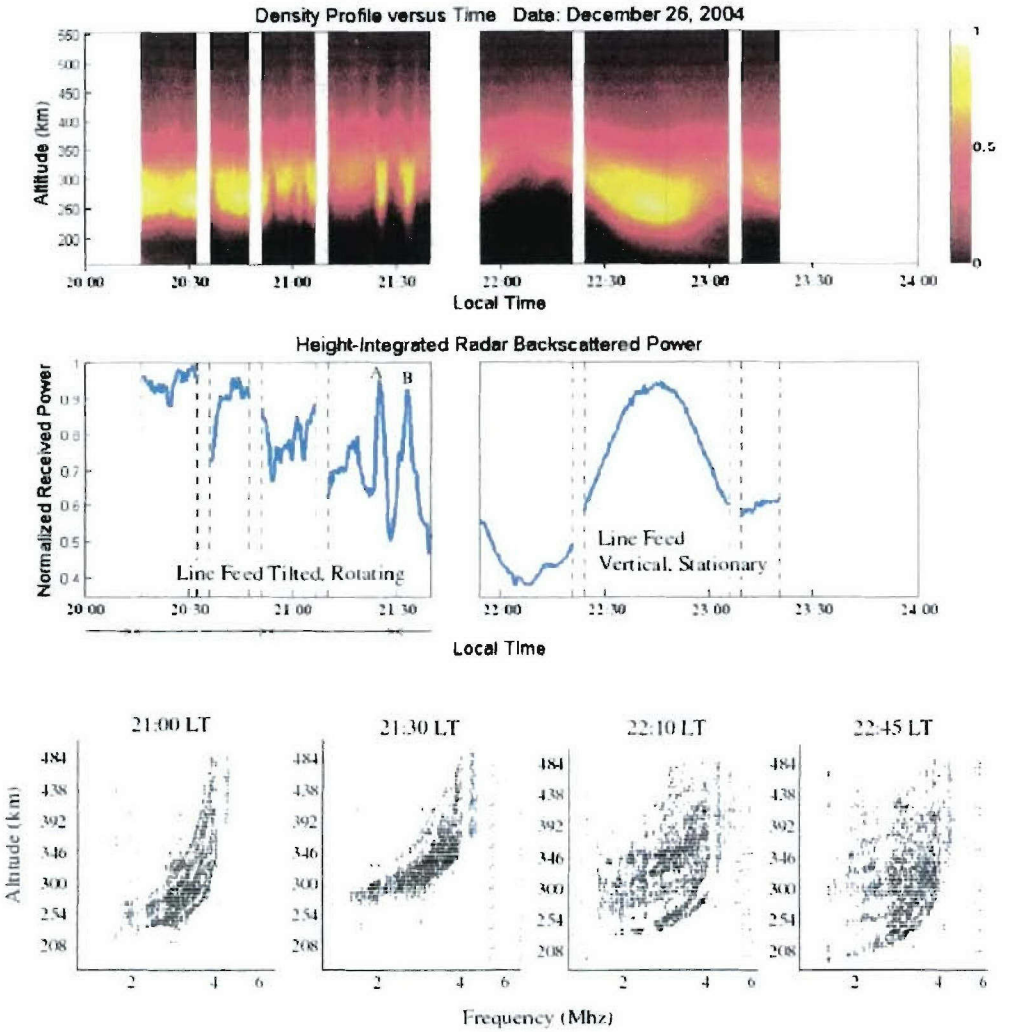

Figure 8. (Top panel) The range-time-intensity (RTI) plot of radar backscatter power recorded on December 26, 2004 from 20:16:21 to 23:20:03 local time (LT). (Middle panel) The corresponding normalized, dimensionless height-integrated radar backscatter power ($\sim$ TEC) as a function of local time. (Bottom panel). Four sampled ionograms recorded during the experiments, to show the excitation of spread F irregularities corresponding to various stages of the naturally occurring ionospheric plasma bubbles.

radar intercepting A then B, with an uncertainty of 14 s. The average radar platform rotation period is 946 s. With this information we can calculate the rotation angles of A and B encounters with respect to the South.

Since (439/946) × 360° = 167.1°, the ISR sampled structure A 12.9° away from due North. Likewise the radar crossed structure B (44/946) × 360 = 16.7° away from due South. The uncertainty is ±5°. At the altitude of 300 km and a tilt angle of 15°, the radius of the circle traced by the radar beam traces is ~80 km. Along the East-West direction, A and B are separated by 80 km × (Sin [16.7°] - Sin [12.9]) = 5.4 km. The estimated East-West component of drift is 5400 m/483 s = 11.2 m/s. This is consistent with the East-West drifts deduced in earlier Arecibo experiments [*Lee et al.*, 1998a]. Because of this small plasma drift, observed dynamic and turbulent ionospheric behavior can be attributed plausibly to the temporal variations of localized ionospheric disturbances detected by the Arecibo radar. The rotating ISR took ~3 minutes to pass cross structures A and B, about 19% of the ISR rotation period. A secant drawn as the third side of an isosceles triangle whose two other sides are cone radii separated by an angle of 19% x 360° (= 69°) has a length of 91 km. Thus, the dense-plasma region is ~ 91 km across. However, since the ISR cone intercepts a narrow cross section of the ionosphere, this must be viewed as a lower limit on the thickness of structure A/B.

(B) Stationary ISR Operations

Having detected an ionospheric structure, we terminated the ISR rotation at 21:39 LT. It took ~15 minutes to bring the line feed to a stationary, vertical position. Stationary line feed operations started at 21:54:29 LT. From 21:54 to 22:10 LT the radar observed a significant ionospheric upwelling and density depletion that appears in Figure 8 to rise and fall. The three density profiles labeled by numbers 1, 2, and 3 in Figure 7(a) were acquired at 21:54:12, 22:00:54 and 22:09:17 LT, respectively. The schematic illustration in Figure 7(b) shows a density depletion developing and moving upward with an apparent velocity of ~100 m/s. Note too in the RTI plot that when the bottomside approached its highest altitude the local plasma became highly structured. Sequentially recorded ionograms support this scenario, showing a large expansion in the altitude range of spread-F echoes, while the height of the F peak remained unchanged. These observations were independently verified in simultaneously recorded ionograms from the nearby Ramey Air Force Base. Figure 9 shows that ionosonde field-of-views at Arecibo and Ramey nearly overlap.

The RTI plot shows that as the ionosphere descend between 22:12 LT and 22:45 LT bottomside structuring vanished. However, the last two ionograms in Figure 8 show that very intense spread F signatures persisted throughout this period. Signs of the bottomside irregularities are evident in the RTI plot especially near 21:10 LT when the F layer was at its highest altitude. Equation (1) suggests that the growth rate for bottomside plasma-density irregularities should increase at higher attitudes where the effective ion-neutral collision rate is low. The fact that spread F did not disappear by 23:45 LT suggests that either the time for plasma descent was quicker than the time for recombination or the irregularities had moved to a different part of the sky observable by the ionosonde, but

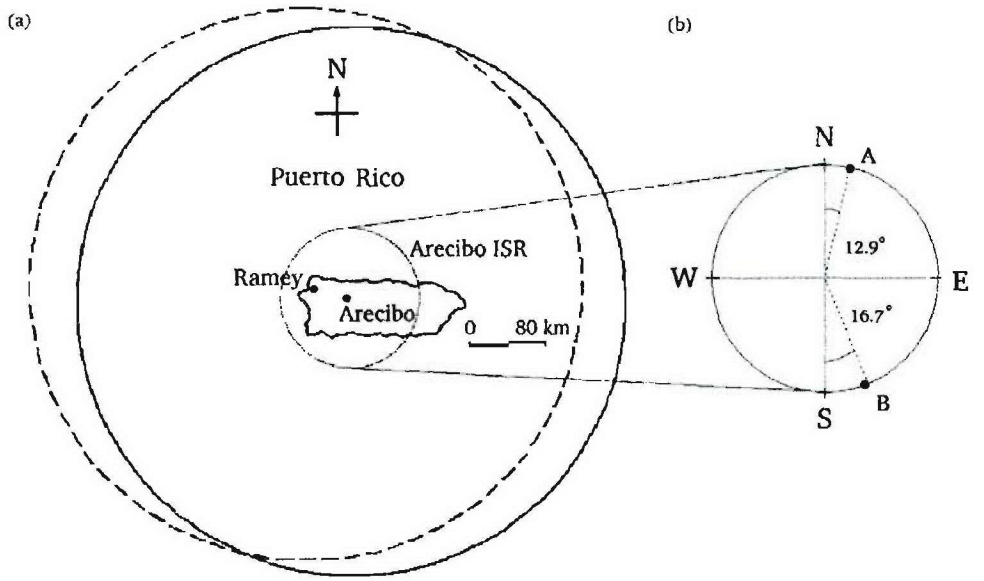

Figure 9. (a) Map of Puerto Rico showing the field of view (FoV) of Ramey ionosonde (dashed line) and Arecibo ionosonde (solid line), at an altitude of 300 km. The dotted line shows the trace cross-section of Arecibo ISR when the beam is rotating and at a maximum angle from the zenith. (b) Arecibo ISR trace cross-section.

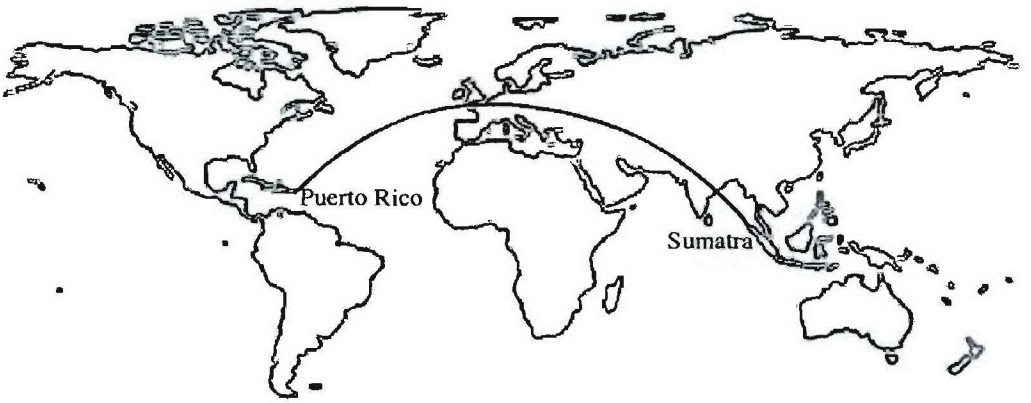

Figure 10. Illustration of tsunami-generated gravity wave propagation along a great circle path between northern Sumatra and Puerto Rico, passing over some land and ocean.

outside the narrow ISR field-of-view. The smooth structure of bottomside plasma directly above Arecibo, evident in the RTI plot at 23:45 LT, suggests that the latter interpretation is more probable.

Discussions and Conclusions

We investigated mid-latitude spread-F phenomenon in experiments conducted in late December 2004, using the 430 MHz radar and the ionosonde at Arecibo Observatory. The tilted and rotating radar beam facilitated finding active regions in the ionosphere above Puerto Rico. During the two periods when the radar beam was stationary very different phenomenologies were detected. On the night of December 25, 2004 (LT) the ionosphere near zenith descended smoothly. Ionograms from the period indicate very weak spread F activity. On the night of December 26 the ionosphere at local zenith rose then fell. Plasma density irregularities in the bottomside produced significant spread F signatures that lasted well after the local ionosphere descended.

Nicolls and Kelley [2005] found experimental evidence for gravity wave seeding of ionospheric plasma irregularities at Arecibo. The causative gravity waves were generated by intense geomagnetic activity at auroral latitudes and propagated primarily in the meridional direction as a train of large-scale traveling ionospheric disturbances (TID). As pointed out in the introduction, geomagnetic conditions were relatively quiet both before and during the period of our experiments. Traces of auroral electrojet indices as well as particle and field measurements from multiple DMSP satellites indicate that geomagnetic activity was low for many hours prior to ISR turn-on. Thus, gravity waves, in the form of traveling ionospheric disturbances (TID), launched by auroral activity appear unlikely throughout the periods of interest. Prevailing clear weather conditions do not indicate the presence of local tropospheric sources of gravity waves.

We note however that the experiments of the second day started about 23 hours after a $M_W = 9.2$ earthquake occurred at 00:57 UT on December 26, 2004 off the west coast of Sumatra, Indonesia. Stevenson [2005] estimated the speed of the tsunami waves on the open Indian Ocean was ~200 m/s. The dual-frequency altimeter on the JASON satellite measured the tsunami's wavelength and amplitude to be ~500 km and 30 to 60 cm [Wilson, 2005]. With these numbers we estimate that the period of the waves as about 42 min.

In the 2001 seismic event, Artru et al. [2005] showed that tsunami-induced gravity waves with typical periods of ~30 minutes can propagate with a vertical- and horizontal-velocity components of order of 50 and 200 m/s, respectively, along great circles between Peru and Japan. The vertical speed estimate suggested that that the gravity wave reached ionospheric altitude in about two and a half hours. Disturbances in the form of TEC structures appeared 22 hours after the earthquake in the ionosphere above Japan at about the same time that tsunami waves reached its shores.

It is interesting to speculate that perhaps gravity waves launched by the tsunami could be responsible for the observed ionospheric disturbances. Unlike the case reported by Artru

et al. [2005] the tsunami waves caused by the Sumatra earthquake in the 2004 seismic event were trapped in Indian Ocean. Obviously, intervening landmasses prevented tsunami waves from reaching the shores of Puerto Rico. We thus expect that the tsunami-generated gravity waves should appear more like discrete rather than a continuous train of TIDs. Figure 10 shows the great circle path between the earthquake's epicenter off the coast of Sumatra (95.78° E, 3.3° N and Puerto Rico (66W, 18.5° N). A path length of ~18,000 km would be traversed in by a signal propagating at a speed of 200 m/s in ~ 25 hours. The time between the earthquake event and the detection of a rising ionosphere by the stationary ISR was about 25 hours. If indeed a tsunami-induced gravity waves traveled from Sumatra to Puerto Rico it would be capable of raising height of the local ionosphere [Nicholls and Kelley, 2005] and seeding the plasma density irregularities and yielding spread F signatures observed above Arecibo between 23:00 - 24:00 LT on December 26, 2004.

Possible evidence for the arrival of tsunami-induced gravity waves over Arecibo may be seen on the RTI plot recorded on December 26, 2004 during the stationary, vertical radar line feed operations between 21:54:29 and 24:00:00 LT. We interpret the apparent rise and fall of the ionospheric F layer primarily as temporal event rather than a spatial structure drifting through the ISR's narrow field-of view. Using the second smaller peak appearing on the RTI around 23:10 LT as a reference, we locate the first peak at about 22:30 LT buried in the downward drifting F layer to estimate the gravity wave period of ~ 40 min. Gravity waves have embedded wind structures that through ion-neutral collisions move ionospheric plasma along and across magnetic field lines. This neutral-plasma coupling can be elucidated in terms of the following ion momentum equation:

$$n_i m_i (\partial/\partial t + \mathbf{V}_i \cdot \nabla) \mathbf{V}_i = -\nabla P_i + n_i m_i \mathbf{g} + n_i e(\mathbf{E} + \mathbf{V}_i \times \mathbf{B}) - n_i m_i \nu_{in}(\mathbf{V}_i - \mathbf{U}_n) \qquad (1)$$

where n_i, m_i, g, e, $\mathbf{V}_i$, P_i, ν_{in}, $\mathbf{U}_n$, **E** and **B** denote ion density, ion mass, gravity, electric charge, ion velocity, ion pressure, ion-neutral collision frequency, neutral wind velocity, and the local electric and magnetic fields, respectively. From Figure 10 it is expected that gravity waves would propagate toward the southwest over Puerto Rico.

In the rest frame of the plasma, the neutral winds would appear to provide an effective electric field $\mathbf{E}_G = - \mathbf{U}_{n\perp} (\nu_{in}/\Omega_i) \times \mathbf{B}$ where $\mathbf{U}_{n\perp}$ is the perpendicular component of the neutral wind velocity with respect to Earth's magnetic field **B** and Ω_i is ion cyclotron frequency. This perturbation neutral wind field creates $\mathbf{E} \times \mathbf{B}$ plasma drifts across the magnetic field. By contrast, the parallel component of the neutral wind velocity $\mathbf{U}_{n\parallel}$ moves plasma along the magnetic field at about the same velocity. Consequently, large-scale plasma redistribution (interchange) is caused by the perturbation neutral velocity due to a gravity wave, as seen in the RTI plot of December 26, 2004 (Figure 8). From Equation (1), one can estimate that the neutral wind velocity $\mathbf{U}_n$ is sufficient to produce the observed effects, if $U_n > g/\nu_{in}$, about a few meters per second in the nighttime F region.

The density depletion seen in Figure 8 is associated with a change of more than 3 TEC units. This is significantly larger than the ~ ± 1 TEC unit effect that Artru et al. [2005] attributed to a tsunami-induced gravity wave crossing the Pacific Ocean.. Furthermore, in the nighttime mid-latitude ionosphere there are no sources of new plasma to "refill" depleted flux tubes. The observed "rising" depleted flux tubes must be view as the consequence of an interchange instability that allowed in plasma rich and plasma poor flux tubes to sit side by side. We noted in RTI/TEC/ionograms of Figure 4 that while the ionosphere appeared to rise, the intensity of spread F increased. The effective ion-neutral collision rate decreases with altitude thus allowing the Rayleigh-Taylor growth rate to increase. After the height of the ionosphere above Arecibo decreased, the intensity of spread F decreased but did not vanish. This reflect two effects:(1) new irregularities formed elsewhere as the gravity wave propagated across the ionosonde field of view, and (2) time scales for diffusion to destroy large-scale irregularities takes several tens of minutes.

In summary, the rotating radar beam in our Arecibo experiments successfully intercepted active ionospheric regions on both nights. Subsequent stationary/vertical transmissions were designed to closely monitor the further development of enhanced ionospheric irregularities created via interchange instabilities. The different ionospheric responses suggests that on December 26 a gravity wave passed Puerto Rico causing plasma within the ISR field of view to rise and fall. Consistent with growth rates for the generalized Rayleigh-Taylor instability, RTI measurements showed bottomside irregularities forming as the local ionosphere approached its maximum height. The continuance of strong spread F signatures after plasma in the ISR field-of-view descended suggests that new irregularities were created as the wave continued to propagate to the southwest. In the absence of other obvious geophysical sources we have examined the possibility the gravity wave responsible for the ionospheric rise and fall above Arecibo was triggered by the December 26, 2004 tsunami as it propagated across the Indian Ocean. Simple kinematic considerations are not inconsistent with our conjecture. Questions about how such a tsunami-induced gravity waves can couple to and propagate global distances in the ionosphere lies well beyond the scope of this report. However, the possibility that seismic events can affect space weather half way around the world on the following day raises a challenge that merits further investigation.

References

Artru, J., V. Ducic, H. Kanamori, P. Lognonne, and M. Murakami, Ionospheric detection of gravity waves induced by tsunamis, *Geophys. I. Int, 160*, 840, 2005.

Basu, B., Generalized Rayleigh-Taylor instability in the presence of time-dependent equilibrium, *J. Geophys. Res.*, 102, 17,305, 1997.

Basu, Su., Sa. Basu, S. Ganguly, and J. A. Klobuchar, Generation of kilometer scale irregularities during the midnight collapse at Arecibo, *J. Geophys. Res.*, *86*, 7607, 1981.

Behnke, R. A., F layer height bands in the nocturnal ionosphere over Arecibo, J.

Geophys. Res., *84*, 974, 1979.

Booker, H. G. and H. W. Wells, Scattering of radio waves by the F region of the ionosphere, *J. Geophys. Res.*, *43*, 249, 1938.

Davis, M. J., and A. V. da Rosa, Traveling ionospheric disturbances originating in the auroral oval during polar substorms, *J. Geophys. Res.*, *74*, 5,721, 1969.

Dewan, E. M., R. H. Picard, R. R. O'Neil, H. A. Gardiner, J. Gibson, J. D. Mill, E. Richards, M. Kendra and W. O. Gallery, MSX satellite observations of thunderstorm-generated gravity waves in mid-latitide infrared images of the upper stratosphere, *Geophys. Res. Lett.*, *25*, 939, 1998.

Eccles, J. V., A simple model of low-latitude electric fields, *J. Geophys. Res.*, *103*, 26,699, 1998.

Huang, C. Y., W. J. Burke, J. S. Machuzak, L. C. Gentile, and P. J. Sultan, DMSP observations of in the topside ionosphere near solar maximum, *J. Geophys. Res.*, *106*, 8,131, 2001.

Kelley, M. C., and M. F. Larsen, Gravity wave initiation of equatorial spread F; A case study, *J. Geophys. Res.*, *86*, 9,087, 1981.

Kelley, M. C., C. E. Seyler, and S. Zargham, Collsional interchange instability 2. A comparison of the numerical simulations with the in situ experimental data, *J. Geophys. Res.*, *92*, 10073, 1987.

Lee, M. C., R. J. Riddolls, W. J. Burke, M. P. Sulzer, E. M. C. Klien, M. J. Rowlands, and S. P. Kuo, Ionospheric plasma bubble generated by Arecibo heater, *Geophys. Res. Lett.*, *25*,579, 1998 (a).

Lee, M. C., R. J. Riddolls, W. J. Burke, M. P. Sulzer, S. P. Kuo, and E. M. C. Klien, Generation of large sheet-like ionospheric plasma irregularities at Arecibo, *Geophys. Res. Lett.*, *25*, 579, 1998 (b).

Lee, M. C., E. M. C. Klien, W. J. Burke, A. X. Zhang, R. J. Riddolls, S. P. Kuo, M. P. Sulzer, and B. Isham, Augmentation of natural ionospheric plasma turbulence by HF heater waves, *Geophys. Res. Lett.*, *26*, 37, 1999.

McClure, J. P., S. Singh, D. K. Bamgboye, F. S. Johnson, and H. Kil, Occurrence of equatorial F region irregularities: Evidence for tropospheric seeding, *J. Geophys. Res.*, *103*, 29,119, 1998.

Meriwether, J.W., J.L. Mirick, M.A. Biodi, F.A. Herero, and C.G. Fesen, Evidence for orographic wave heating in the equatorial thermosphere at solar maximum, *Geophys. Res. Lett.*, 23, 2177, 1996

Nicolls, M.J. and M.C. Kelley, Strong evidence for gravity wave seeding of an ionospheric plasma instability, *Geophys. Res. Lett., 32*, 679, 2005.

Ossakow, S.L., Spread-F theories --- a review, *J. Atmos. Terr. Phys., 43*, 437, 1981.

Rich, F. J., and M. Hairston, Large-scale convection patterns observed by DMSP, *J. Geophys. Res., 99*, 3827, 1994.

Singh, S., F. S. Johnson, and R. A. Power, Gravity wave seeding of equatorial plasma bubbles, *J. Geophys. Res., 102*, 7399, 1997.

Stevenson, D., Tsunami and earthquakes: What physics is interesting?, *Phys. Today*, 58, 10, 2005.

Sultan, P. J., Linear theory and modeling of the Rayleigh-Taylor instability leading to the occurrence of equatorial spread F, *J. Geophys. Res.*, 101, 26,875, 1996.

Tsunoda, R. T., R. C. Livingston, J. P. McClure, and W. B. Hanson, Equatorial plasma bubbles: Vertically elongated wedges from the bottomside F layer, *J. Geophys. Res., 87*, 9171, 1982.

Wilson, M., Modeling the Sumatra-Andaman earthquake reveals a complex, nonuniform rupture, Wilson, M., Modeling the Sumatra-Andaman earthquake reveals a complex, nonuniform rupture, *Phys. Today*, 58, 19, 2005.

Zalesak, S. T., and S. L. Ossakow, On the prospect for artificially inducing equatorial spread *F*, Memo. Rep. 4899, Nav. Res. Lab., Washington, D.C., Sept. 1982.